Cavity optomechanics in a levitated helium drop

L. Childress,[1,2] M. P. Schmidt,[3] A. D. Kashkanova,[1] C. D. Brown,[1] G. I. Harris,[1] A. Aiello,[3,4] F. Marquardt,[3,4] and J. G. E. Harris[1,5,6]

[1]*Department of Physics, Yale University, New Haven, Connecticut 06520, USA*
[2]*Department of Physics, McGill University, 3600 Rue University, Montreal, Quebec, Canada H3A 2T8*
[3]*Institute for Theoretical Physics, Department of Physics, University of Erlangen-Nürnberg, Staudtstrasse 7, 91058 Erlangen, Germany*
[4]*Max Planck Institute for the Science of Light, Staudtstr. 2, 91058 Erlangen, Germany*
[5]*Department of Applied Physics, Yale University, New Haven, Connecticut 06520, USA*
[6]*Yale Quantum Institute, Yale University, New Haven, Connecticut 06520, USA*

(Received 29 August 2017; published 29 December 2017)

We describe a proposal for a type of optomechanical system based on a drop of liquid helium that is magnetically levitated in vacuum. In the proposed device, the drop would serve three roles: its optical whispering-gallery modes would provide the optical cavity, its surface vibrations would constitute the mechanical element, and evaporation of He atoms from its surface would provide continuous refrigeration. We analyze the feasibility of such a system in light of previous experimental demonstrations of its essential components: magnetic levitation of mm-scale and cm-scale drops of liquid He, evaporative cooling of He droplets in vacuum, and coupling to high-quality optical whispering-gallery modes in a wide range of liquids. We find that the combination of these features could result in a device that approaches the single-photon strong-coupling regime, due to the high optical quality factors attainable at low temperatures. Moreover, the system offers a unique opportunity to use optical techniques to study the motion of a superfluid that is freely levitating in vacuum (in the case of ^{4}He). Alternatively, for a normal fluid drop of ^{3}He, we propose to exploit the coupling between the drop's rotations and vibrations to perform quantum nondemolition measurements of angular momentum.

DOI: 10.1103/PhysRevA.96.063842

I. INTRODUCTION

Optomechanical systems [1] have been used to demonstrate quantum effects in the harmonic motion of macroscopic objects over a very broad range of physical regimes. For example, quantum optomechanical effects have been observed in the motion of objects formed from all three states of matter (solid [2], gas [3], and liquid [4]), at temperatures ranging from cryogenic to room temperature [5], with effective mass as large as ∼100 nanograms [6], and with resonance frequencies ranging from kHz to GHz. Despite rapid progress, a number of important goals in this field remain outstanding, for example, generating highly nonclassical states of motion with negative quasiprobability distributions or which violate a Bell-type inequality (even without postselection), efficiently transferring quantum states between microwave and optical frequencies, and observing quantum effects in the motion of objects massive enough to constrain theories of quantum gravity [7–9]. Access to these phenomena may be facilitated by devices with reduced optical and mechanical loss, increased optomechanical coupling, and increased mass, motivating exploration of novel systems with capabilities complementary to existing devices. In addition, new regimes and qualitatively new forms of optomechanical coupling may be accessed by developing systems in which the mechanical degrees of freedom are not simply the harmonic oscillations of an elastic body. In this work, we will show that a levitated drop of superfluid helium will be a most promising platform that combines many of these desired features and offers novel possibilities.

To date, most optomechanical devices are realized by using solid objects (e.g., mirrors, waveguides, or electrical circuits) to confine modes of the electromagnetic field, and ensuring that these confined modes couple to the harmonic motion of a solid object. These devices' performance is determined in part by the properties of the solids from which they are formed. For example, the material's mechanical and electromagnetic loss are important parameters, as is the material's compatibility with fabrication techniques. For this reason, high-quality dielectrics are typically employed in devices using optical fields, while superconductors are typically employed in devices using microwave fields.

Most solid-based optomechanical devices must be placed in direct contact with their solid surroundings, both to support them against Earth's gravity and to provide thermal anchoring. This contact can negatively affect the device's performance,

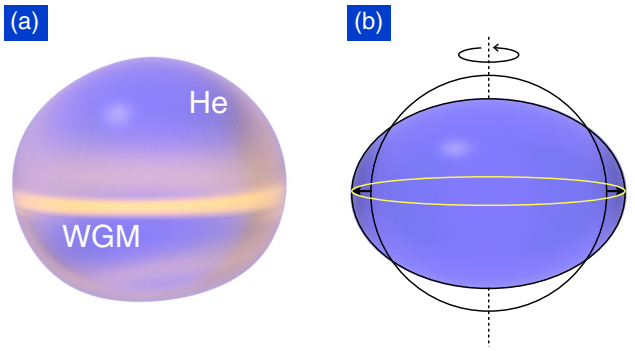

FIG. 1. (a) Schematic illustration of a levitated helium drop containing an optical whispering-gallery mode (WGM), whose optical path length is modified by the surface vibrations. (b) Rotation of the drop leads to an equatorial bulge, which also modifies the WGM's path length.

as it represents a route for mechanical loss. It may also be problematic if the contact is not able to provide effective cooling (i.e., to counteract heating from electromagnetic absorption in the device), as elevated temperatures tend to obscure quantum effects.

If the mechanical element is a solid object that is levitated in vacuum (e.g., using optical or magnetic forces) [10–17], the absence of direct contact can result in very low loss for some mechanical degrees of freedom (particularly the object's center of mass). However, the absence of direct contact also precludes effective cooling of the element. This is particularly important given the nonzero optical absorption of conventional materials and the high optical powers typically required for levitation and/or read out of the object's motion. As a result, solid objects levitated in vacuum have operated at elevated bulk temperatures (although some degrees of freedom may still be cooled to very low effective temperatures).

In contrast to solid objects, atomic gases may be levitated and trapped in vacuum at very low temperatures. This is due to two important features of atomic systems. First, the gas is heated only via the atoms' spontaneous emission (which can be minimized by using laser fields that are far detuned from the atomic transitions). Second, the atoms can all be kept cold by laser cooling and evaporation. When a cloud of ultracold atoms is trapped inside an optical cavity, its center-of-mass motion (or some collective mode of the gas) can detune the cavity, leading to an optomechanical interaction [18,19]. This interaction may be quite strong, as the small number of atoms can be compensated by the cloud's large zero point motion and by adjusting the detuning between the atomic transition and the cavity. Ultracold atom-based optomechanical devices have achieved optomechanical figures of merit and demonstrated quantum optomechanical effects that are competitive with state-of-the-art solid-based devices. However, the effective mass of atom-based devices is likely to remain several orders of magnitude lower than solid-based devices, making them less promising for foundational tests.

Recently, optomechanical devices that employ liquids have been demonstrated. These can be realized by supporting a drop of liquid [20] so that its free surface confines an electromagnetic mode in the form of an optical whispering-gallery mode (WGM). In this case, the drop serves as both the optical cavity and the mechanical element, as the drop's surface oscillations tend to detune the drop's optical WGMs. Devices based on this approach have been demonstrated at room temperature and with the drops mechanically anchored (rather than levitating). However, the relatively high mechanical loss in room-temperature fluids has precluded them from accessing quantum optomechanical effects.

Liquid-based optomechanical devices can also be realized by filling [21–24] or coating [25] a solid electromagnetic cavity with a fluid. In this case only the mechanical degree of freedom is provided by the fluid, for example, as a density wave or surface wave that detunes the cavity by modulating the overlap between the liquid and the cavity mode. This approach has been used at cryogenic temperatures with superfluid ^{4}He serving as the liquid [22–26].

Liquid He has a number of properties that make it appealing for optomechanical devices. Its large band gap ($\sim$19 eV), chemical purity, and lack of structural defects should provide exceptionally low electromagnetic loss. In its pure superfluid state, the viscosity that strongly damps other liquids is absent. The mechanical loss arising from its nonlinear compressibility varies with temperature T as T^4, and so is strongly suppressed at low T. In addition, its thermal conductivity at cryogenic temperatures is exceptionally large.

To date, optomechanical devices based on superfluid-filled cavities have reaped some advantage from these features (including the observation of quantum optomechanical effects [4]). However, the need to confine the superfluid within a solid vessel has undercut many of the advantages offered by superfluid helium. This is because direct contact between the superfluid and a solid object provides a channel for mechanical losses (i.e., radiation of mechanical energy from the superfluid into the solid) and heating (due to electromagnetic absorption in the solid).

In this paper, we propose a type of optomechanical device that is intended to combine advantages from each type of device described above. Specifically, we consider a millimeter-scale drop of superfluid He that is magnetically levitated in vacuum (Fig. 1). Magnetic levitation would provide high-quality optical WGMs and high-quality mechanical modes by confining the optical and mechanical energy entirely within the superfluid. Despite being levitated in vacuum, the drop would be able to cool itself efficiently by evaporation, thereby compensating for any residual heating.

In addition to offering these technical improvements, this approach would provide access to qualitatively different forms of optomechanical coupling. A levitated drop of ^{3}He in its normal state would retain the low optical loss and efficient cooling of the superfluid drop, but would experience viscous damping of its normal modes of oscillation. However, its rigid body rotation (which is not directly damped by viscosity) would couple to the drop's optical WGMs. The coupling arising in such an "optorotational" system is distinct from the usual optomechanical coupling, with important consequences for quantum effects.

Besides establishing an optomechanics platform, the proposed system may also help address long-standing questions regarding the physics of liquid helium. For example, a levitated drop of ^{4}He may contain a vortex line [27,28] which deforms the drop shape and hence detunes the optical WGMs, providing a probe of vortex dynamics. Alternately, optical measurements of a levitated drop could probe the onset and decay of turbulence in a system without walls.

Most of the essential features of the proposed device have been demonstrated previously, albeit in disparate settings. These include the magnetic levitation and trapping of mm-scale and cm-scale drops of superfluid helium [29,30], the characterization of these drops' surface modes [31] for $T > 650$ mK, the observation of evaporative cooling of He drops [32] in vacuum, and the observation of high-finesse optical WGMs in liquids such as ethanol [33–35] and water [36] (at room temperature) and in liquid H_2 [37,38] (at $T \sim 15$ K). This paper uses these prior results to estimate the optomechanical properties of a levitated drop of liquid He, including the possible coupling to rotational motion. The discussion presented here is relevant for both ^{3}He and ^{4}He, except where noted otherwise.

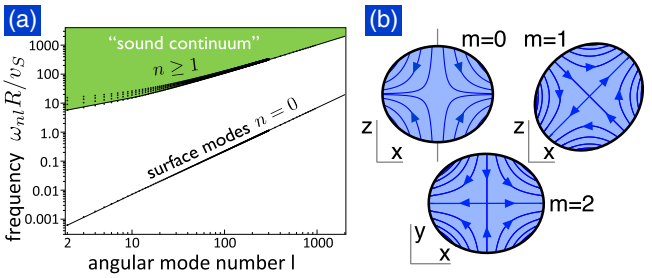

FIG. 2. (a) Vibrational modes of a spherical drop, with radial index n and angular index l; the surface modes $n = 0$ are separated from the bulk continuum ($n \geqslant 1$). Points represent the discrete mode frequencies and solid lines represent the analytical expressions for the $n = 0$ and $n = 1$ mode frequencies. (b) Illustrations of the velocity profiles for $l = 2$ surface modes of different azimuthal number m.

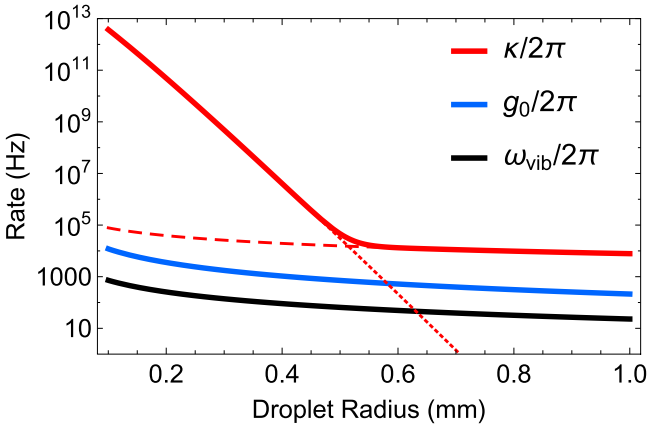

FIG. 3. Mechanical frequency ω_{vib} for a $l = 2$ mode, the optical decay rate κ, and the optomechanical coupling constant g_0, all as a function of drop radius (for $T = 300$ mK and $\lambda = 1$ μm). The dashed curve shows optical loss due to scattering from thermal surface fluctuations; the dotted curve shows radiative loss due to surface curvature.

II. OPTOMECHANICAL COUPLING IN A HELIUM DROP

We begin by discussing the vibrational modes of the drop and deriving their optomechanical coupling to the optical WGMs. Note that WGMs in spherical (and near-spherical) dielectrics are discussed extensively in the literature [39], so we do not review their properties here.

A. Vibrational modes

The vibrational modes of a helium drop can be calculated by solving the linearized hydrodynamic equations (Fig. 2). The angular dependence of each mode is given by a spherical harmonic $Y_{l,m}(\theta,\phi)$ (where l and m index the mode's total angular momentum and its projection on the z axis). The radial dependence of each mode can be written in terms of spherical Bessel functions $j_n(kr)$ (where k is the mode's wave number and n determines the number of radial nodes). The physical nature of these modes falls into two classes.

(i) Low-frequency surface modes (ripplons), whose restoring force is provided by surface tension. These have frequency $\omega_l = \sqrt{l(l-1)(l+2)\sigma/(\rho R^3)}$ [40] for the $2l+1$ degenerate modes at any given angular mode number $l = 2,3,\ldots$, where R is the radius of the drop, ρ is its density, and σ is its surface tension. For a ^{4}He drop of radius $R = 1$ mm, the $l = 2$ mode whose optomechanical coupling we will analyze has a frequency of $\omega_2 = 2\pi \times 23$ Hz $\equiv \omega_{vib}$.

(ii) Sound modes, whose restoring force is provided by the elastic modulus. The frequency of these modes depends on the indices n and l [41,42]. These include "breathing" modes and acoustic whispering-gallery modes, among others. Their frequencies scale with v_s/R, where v_s is the speed of sound in liquid He. For the example of a ^{4}He drop with $R = 1$ mm, the lowest-frequency compressional mode oscillates at $2\pi \times$ 120 kHz.

In the present work we focus on the surface modes, specifically the lowest nontrivial modes (quadrupole deformations, $l = 2$). These couple most strongly to the optical WGMs.

B. Optomechanical coupling to surface modes

The single-quantum optomechanical coupling can be found from the optical WGM detuning produced by the surface mode's quantum zero-point fluctuation amplitude. To calculate this amplitude, we note that the surface deflection $\delta R(\theta,\varphi)$ can be decomposed in terms of the surface modes as $\delta R = \sum_{l,m} X_{l,m} Y_{l,m}(\theta,\varphi)$, where $X_{l,-m} = X^*_{l,m}$ are the time-dependent mode amplitudes. The spherical harmonics $Y_{l,m}$ are normalized such that $\int d\Omega\, |Y_{l,m}|^2 = 1$.

The potential energy of the modes is determined by surface tension σ. For the $l = 2$ modes of interest here, the increase of surface area is given (to lowest order) by $2\sum_m |X_m|^2$. We note that in order to obtain this result, care needs to be taken to preserve the volume of the drop by adjusting the radius (i.e., the $l = 0$ monopole contribution to δR) [43]. Focusing on the $l = 2, m = 0$ mode, we then equate the average potential energy $2\sigma\langle X_0^2\rangle$ to half of the zero-point energy $\hbar\omega_{vib}/4$. From this, we find the zero-point fluctuation amplitude of the $m = 0$ surface mode, as well as the change of radius at the drop's equator:

$$X_{0,\mathrm{ZPF}} = \sqrt{\frac{\hbar\omega_{vib}}{8\sigma}}, \quad \delta R_{\mathrm{ZPF}} = \sqrt{\frac{5}{16\pi}} X_{0,\mathrm{ZPF}}. \tag{1}$$

Again, for a drop of ^{4}He with $R = 1$ mm, this is $X_{0,\mathrm{ZPF}} = 2.2$ fm.

Each optical WGM in the drop is specified by the indices $\tilde{l}$, $\tilde{m}$, and $\tilde{n}$ (which specify the WGM's total angular momentum, its projection along the z axis, and the number of radial nodes, respectively). The WGM that lies closest to the drop's equator (i.e., with $\tilde{l} = \tilde{m}$) has an optical path length that is proportional to the drop's equatorial circumference. As a consequence, we find $g_0 = \omega_{\mathrm{opt}}\delta R_{\mathrm{ZPF}}/R$ for the bare optomechanical coupling between an equatorial optical whispering-gallery mode and the $l = 2, m = 0$ surface mode. For $\lambda = 1$ μm and $R = 1$ mm, this amounts to $g_0 = 2\pi \times 213$ Hz (see Fig. 3).

We note that the optical frequency of the equatorial WGM couples linearly only to the surface mode with $m = 0$. All $m \neq 0$ vibrational surface modes will be restricted to (considerably weaker) higher-order coupling.

Optical WGMs with arbitrary $(\tilde{l},\tilde{m})$ [44] also couple linearly to the $l = 2, m = 0$ mechanical mode, with coupling rates

$$g_0^{(\tilde{l},\tilde{m})} = \omega_{\rm opt}\frac{\delta R_{\rm ZPF}}{R}\frac{1}{2}\left[3\frac{\tilde{m}^2}{\tilde{l}(\tilde{l}+1)} - 1\right]. \quad (2)$$

WGMs propagating near the equator (i.e., with large $\tilde{m}$) have the usual sign of the coupling (a decrease of optical frequency on expansion), while those with small $\tilde{m}$ have the opposite sign. In a ray-optical picture, they travel along great circles passing near the pole, and feel an overall reduction of path length when the drop's equator expands.

The preceding discussion applies strictly to a perfectly spherical drop. In practice, the magnetic fields used to counteract the pull of gravity tend to distort the drop's shape [45]. A rotating drop will also experience distortion due to centrifugal forces. Such distortions break the degeneracy of the optical WGMs. Equation (2), with $\delta R_{\rm ZPF}$ replaced by the change of radius δR, can also be used to estimate the impact of this distortion on the optical WGMs. A family of modes with any given $\tilde{l}$ splits into $\tilde{l}+1$ distinct frequencies (as modes with given $|\tilde{m}|$ remain degenerate), with the frequency shift $\propto\tilde{m}^2$. In the case of modes with $\lambda = 1\ \mu$m, $R = 1$ mm scenario and a distortion $\delta R/R \sim 1\%$, the originally degenerate multiplet would split into a band with ~THz bandwidth, far larger than the vibrational frequencies we consider. Indeed, the bandwidth of frequencies produced from each $\tilde{l}$ manifold would exceed the free spectral range of the WGMs by more than an order of magnitude, meaning that optical modes with differing $\tilde{l}$ could undergo avoided crossings for certain values of the distortion.

III. MECHANICAL AND OPTICAL QUALITY FACTORS

A. Damping of mechanical modes

As described in the Introduction, the combination of superfluidity and magnetic levitation should strongly suppress some sources of mechanical damping. Here we consider the two mechanisms which are expected to dominate the energy loss from the mechanical modes of a ^{4}He drop. The first is due to damping by the He gas surrounding the drop and the second is the exchange of mechanical energy between the drop's mechanical modes (i.e., mediated by its mechanical nonlinearity). Both of these processes are strongly temperature dependent.

At sufficiently high temperatures, the vapor surrounding the drop and the thermal excitations within the drop are dense enough to be described as hydrodynamic fluids. Experiments in this regime measured the quality factor $Q_{\rm mech}$ of the $l = 2$ surface modes for a ^{4}He drop of radius $R = 2$ mm for $0.65\ {\rm K} \leqslant T \leqslant 1.55\ {\rm K}$ [46]. The measured $Q_{\rm mech}(T)$ was in good agreement with calculations based on a hydrodynamic treatment of the three fluids (i.e., the superfluid, normal fluid, and vapor) [47]. Within this temperature range, $Q_{\rm mech}$ reached a maximum value (~1200) for $T \sim 1.2$ K (see Fig. 4). At higher T, the decrease in $Q_{\rm mech}$ is due to the higher vapor density. At lower T the decrease in $Q_{\rm mech}$ is due to the increasing dynamic viscosity of ^{4}He.

The counterintuitive increase in viscosity with decreasing T reflects the increasing mean free path Λ of the thermal phonons within the drop. Since Λ is proportional to T^{-4} [48,49], at still lower temperatures the drop will enter a new regime in which $\Lambda > R$. In this regime the hydrodynamic description fails and $Q_{\rm mech}$ is expected to increase again. Some support for this picture can be found in the measurements of Refs. [50,51]. For a $R = 1$ mm drop, this regime should occur for $T < 0.4$ K.

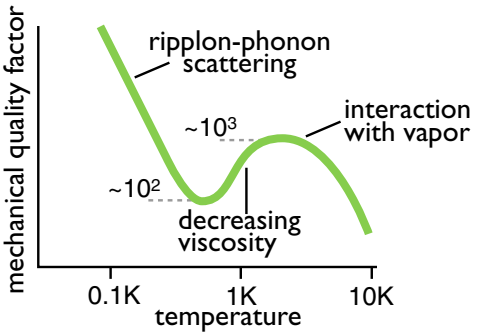

FIG. 4. Qualitative sketch of the expected temperature dependence for the mechanical quality factor $Q_{\rm mech}$ of $l = 2$ surface modes in a $R = 1$ mm ^{4}He drop, with indication of different regimes. In the regime of viscous damping, the viscosity of the normal component *drops* with increasing temperature, which leads to nonmonotonic behavior of the quality factor.

At these low temperatures, the dominant loss mechanism for the surface waves (ripplons) is ripplon-phonon-phonon scattering, in which a thermally excited bulk phonon scatters off the ripplon and is Doppler shifted, carrying away energy. This effect has been studied experimentally and theoretically in Ref. [52], with a resulting estimate for the $Q_{\rm mech}$ of a surface wave traveling on a plane surface:

$$\frac{1}{Q_{\rm mech}} = \frac{\pi^2}{90}\frac{\hbar k}{\rho\omega}\left(\frac{k_B T}{\hbar v_s}\right)^4. \quad (3)$$

Here ω is the surface mode frequency, k is its wave number, ρ is the density, and v_s is the sound velocity.

While our proposal focuses on mechanical modes of ^{4}He drops, for completeness we also note the mechanical losses of ^{3}He drop surface modes. For a normal-fluid ^{3}He drop, one can apply Chandrasekhar's result for the viscous damping [53], according to which $1/Q_{\rm mech} = \mu(l-1)(2l+1)/(\omega R^2\rho)$. Here μ is the dynamic viscosity and ρ is the density. For $T = 1$ K, where $\mu = 30\ \mu$P, a 1 mm drop would have $l = 2$ surface modes with $Q_{\rm mech} \approx 70$, and the quality factor would decrease approximately as $Q_{\rm mech} \propto T^2$ at lower temperatures [54,55]. For $T \lesssim 1$ mK, a ^{3}He drop would become superfluid; however, this temperature range is not likely to be accessed via the cooling methods considered here.

B. Damping of optical whispering-gallery modes

Light confined within a WGM may experience loss due to radiation from the evanescent portion of the mode, scattering from surface roughness or bulk defects, or absorption by the host material or its impurities [39]. Here we consider the contributions of each of these mechanisms to the quality factor of the optical WGMs in a levitated drop of liquid helium.

Optical WGMs have been studied in drops of several different types of liquid. Pioneering experiments by the Chang group [33,35,56] focused on WGMs in freely falling drops

of ethanol and water and found optical $Q_{\rm opt}$ as high as 10^8. Measurements of WGMs in suspended drops of oil show $Q_{\rm opt} = 1.7 \times 10^8$ [20]. Pendant drops of cryogenic liquid H_2 [37,38] demonstrated $Q_{\rm opt} = 4.2 \times 10^9$.

In comparison with these materials, liquid He should offer reduced absorption. This is because He is monoatomic (removing the possibility of inelastic light scattering from bond stretching or other molecular degrees of freedom), has a large gap for electronic excitations ($\sim$19 eV), and is free of chemical impurities and surface adsorbates.

Liquid He posesses an unusually low index of refraction ($n \sim 1.028$), which would lead to increased radiative loss at fixed R and λ. However, radiative loss from a spherical resonator decreases exponentially [39] with R/λ. As a result, even with the small refractive index of He, radiative loss becomes negligible in mm-scale drops (see Fig. 3).

Surfaces defined by surface tension are typically very smooth. Nevertheless, thermally excited ripplons will result in an effective surface roughness. As described below, we expect this will be the dominant loss mechanism. To analyze this mechanism we assume that the random thermal surface deformation is essentially frozen during the lifetime of the optical WGM. Furthermore, we only consider ripplon modes with wavelengths small compared to R. In this case the Fourier transform $\tilde{G}(k)$ of the spatial correlation function of surface deflections can be approximated by the known result for a planar surface, $\tilde{G}(k) = 2\pi k_B T/\sigma|k|$, where σ is the surface tension. Adapting an analysis for planar waveguides with a disordered surface [57], the WGM loss rate (via outscattering) is

$$\frac{1}{Q_{\rm opt}} \approx \Phi(0)^2(\epsilon-1)^2\frac{k_0^2}{8\pi}\int_0^\pi \tilde{G}(k-k_0\cos\theta)d\theta. \qquad (4)$$

Here k_0 is the optical WGM's vacuum wave number and $\epsilon = 1.057$ is the dielectric constant of helium. $\Phi(y)$ is the normalized transverse mode shape [$\int \Phi(y)^2 dy = 1$], such that $\Phi(0)^2$, evaluated at the surface, is roughly the inverse extent of the mode. Following Ref. [58] and considering TE modes only, we take $\Phi(0)^2 \approx 2\epsilon/[R(\epsilon-1)]$ as an upper estimate, eventually obtaining $Q_{\rm opt} \approx 2R/(\pi k_0\sqrt{\epsilon-1})(\sigma/k_B T)$ as a lower bound for $Q_{\rm opt}$. Applying this approach to liquid ^{4}He at $T = 300$ mK, with $\sigma = 3.75 \times 10^{-4}$ N/m, and $\lambda = 1$ μm gives $Q_{\rm opt} \sim 4 \times 10^{10}$ for a drop with $R = 1$ mm. For ^{3}He, the surface tension and the resulting Q are both about 2.5 times lower.

At present there are no experiments on He drops with which to compare this estimate. However, applying this analysis to the liquid H_2 drops of Refs. [37,38], gives $Q_{\rm opt} \sim 2 \times 10^8$, i.e., it underestimates $Q_{\rm opt}$ by roughly an order of magnitude. This may reflect the fact that the ripplon modes evolve during the WGM lifetime, averaging out some of the effective roughness.

We estimate other scattering mechanisms to be significantly less important: Brillouin scattering from thermal density fluctuations inside the drop [59,60] should give $Q_{\rm opt} > 10^{13}$ and Raman scattering from rotons should be even weaker (following Ref. [61]).

C. Summary of parameters

Based on the estimates above, the most important optomechanical parameters for a drop of ^{4}He with $R = 1$ mm are summarized in Table I (assuming $T = 300$ mK).

TABLE I. Optomechanical parameters.

$\omega_{\rm vib}/2\pi$	$Q_{\rm mech}$	$Q_{\rm opt}$	$g_0/2\pi$
23 Hz	$>10^3$	$>10^{10}$	213 Hz

Notably, this system enters the previously unexplored regime where $g_0 > \omega_{\rm vib}$. While our estimate for $Q_{\rm opt}$ gives an optical linewidth that is only $\sim$40 times larger than the optomechanical coupling rate, the same "frozen-deformation" approximation underestimates the quality factor of hydrogen drops by a factor of 20. Moreover, at lower temperatures, $Q_{\rm opt} \propto 1/T$ increases yet further. The levitated helium drop is thus likely to approach the single-photon strong-coupling regime.

D. Evaporative cooling

The temperature of an optomechanical device is typically set by the competition between optical absorption (which leads to heating) and the device's coupling to a thermal bath (which allows this heat to be removed). For levitated solids, the heat removal process is inefficient, as it occurs primarily via blackbody radiation, resulting in elevated temperatures for even moderate optical power. In contrast, a levitated liquid may also cool itself via evaporation. As described below, evaporation provides an effective means for maintaining the drop temperature well below 1 K. However, evaporation also couples the drop's radius R to its temperature T. Since many of the device's relevant parameters (such as the resonance frequencies and quality factors of the optical and mechanical modes) depend on both R and T it is important to have a quantitative model of the evaporation process.

Evaporative cooling of helium droplets has been studied both experimentally and theoretically. Experiments to date have used μm- and nm-scale droplets that are injected into a vacuum chamber. In the $\sim$ms time before the droplets collide with the end of the vacuum chamber they are found [32] to reach $T \sim 370$ mK (150 mK) for ^{4}He (^{3}He). This cooling process can be understood by considering how energy loss—given by the latent heat per atom $[\Delta E(T)]$ times the evaporation rate $\Gamma(N,T)$ (atoms/s)—leads to cooling according to the heat capacity $C(N,T)$ of the droplet: $\frac{dT}{dt} = -\Gamma(N,T)\Delta E(T)\frac{1}{C(N,T)}$, where the total number N of atoms in the drop decreases as $\frac{dN}{dt} = -\Gamma(N,T)$. Simultaneous solution of the differential equations yields the cooling dynamics. Theoretical models valid in the low-T, low-N limit have successfully explained the experiments [62]. They used an Arrhenius law for the evaporation rate $\Gamma \propto NT^2 e^{-E_0/k_B T}$ with $E_0 = \Delta E(0) = k_B \times 7.14$ K (2.5 K) for ^{4}He (^{3}He), and considered only ripplon (for ^{4}He) or free Fermi gas (for ^{3}He) contributions to the heat capacity of the drop.

To model the full range of temperatures attained during cooling, and to account for phonon contributions to the heat capacity (needed for large-N drops of ^{4}He), we use primarily measurement-based values [63] of latent heat ΔE, vapor pressure P (which determines the evaporation rate via $\Gamma \approx 4\pi R^2 P/\sqrt{2\pi m k_B T}$ assuming unit accommodation coefficient), and specific heat [64–67]. Figure 5(a) shows

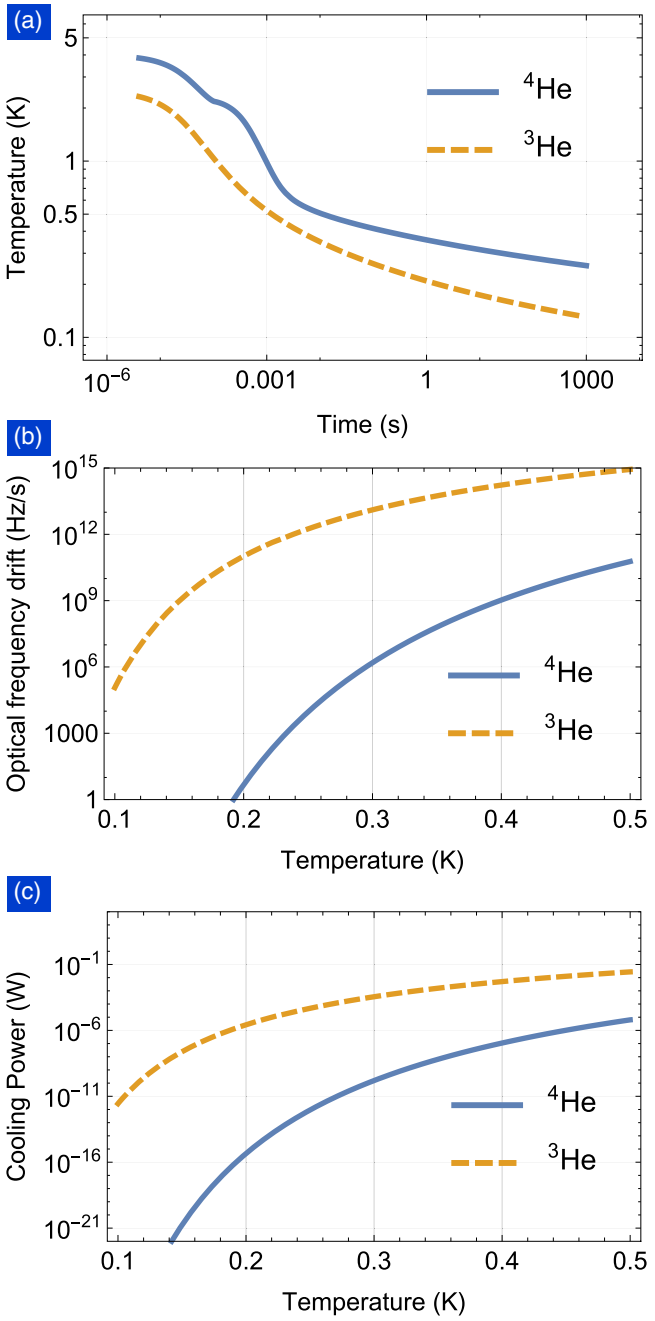

FIG. 5. Evaporative cooling of the helium drop. (a) Evolution of temperature as a function of time for drops with an initial radius $R = 1$ mm (which decreases by about 10% during cooling). Note the logarithmic time scale; the physically relevant times are those above 1 s; lower times depend on the detailed experimental protocol. (b) Rate of change of the whispering-gallery mode resonance frequency, due to the decrease of radius by continuous evaporation, for a $\lambda = 1$ μm mode of a $R = 1$ mm drop. (c) Cooling power $\Delta E\,\Gamma$, displayed as a function of temperature, for $R = 1$ mm. Blue: ^{4}He; dashed orange: ^{3}He.

the expected temperature $T(t)$ for ^{4}He and ^{3}He drops with an initial radius of 1 mm, cooled from 4.0 K and 2.5 K, respectively. Because ^{3}He has a higher vapor pressure, it cools more effectively: for ^{4}He (^{3}He), the drop temperature reaches ∼350 mK (∼200 mK) after ∼1 s evaporation time and slowly cools to ∼290 mK (∼150 mK) after ∼1 min. The complete cooling process shrinks the radius of both types of drops by about 10%.

In the absence of any heat load [as assumed for the simulation shown in Fig. 5(a)], T will continue to decrease, although over impractically long time scales. In an actual experiment we expect a finite heat load on the drop, which will result in T asymptoting to a finite value. The asymptotic value of T will determine the quality factor of the optical and mechanical modes (as described above). It will also set the (constant) rate at which R will drift during any experiment. This drift in R will not result in any appreciable change in the mechanical mode frequencies; however, the drift in the optical mode frequency will need to be tracked, e.g., by standard laser-locking techniques [see Figs. 5(b) and 5(c)].

For a ^{4}He drop with $R = 1$ mm, the optical drift rate is $\sim 10^{16}$ Hz/s per watt of dissipated power (and is ∼4× larger for ^{3}He because of the lower binding energy and density of ^{3}He). To estimate the likely heatload on the drop, we note that Brillouin scattering in the optical WGM [29] should result in absorption of $<10^{-10}$ of the incident laser power (for $\lambda = 1$ μm). Assuming an input power ∼μW, this would result in an optical drift rate of only ∼Hz/s.

IV. ROTATIONS

A. Towards quantum nondemolition measurements of rotation

One of the unique characteristics of fluid drops, as opposed to solid dielectric spheres, is the possibility to optically measure and possibly even control rotations, via the deformation of the rotating drop. Rotational motion represents a low-energy excitation that is not equivalent to a harmonic oscillator, and so offers access to quantum phenomena that are qualitatively distinct from those typically studied in cavity optomechanics. The rotational motion of a levitated liquid differs from that of a levitated solid (described in Refs. [68–75]) in several important respects. These include the liquid's electromagnetic and mechanical isotropy (which should more closely approximate free rotation),the independence between the liquid's external shape and its rotation, and, in the case of superfluid ^{4}He, dissipationless nonrigid body rotational motion.

The rotational motion of ^{4}He is qualitatively different from that of ^{3}He. For the temperatures relevant here (∼300 mK), ^{4}He is a pure superfluid and so its rotation is determined by the presence of vortices, each with quantized circulation. The angular momentum associated with each vortex is $N\hbar$ (where N is the number of atoms in the drop); thus the drop's angular momentum can only change in relatively large discrete steps. In practice, this will ensure that the number of vortices is constant at low temperatures. Nevertheless, a drop with a fixed number of vortices will still possess nontrivial dynamics owing to the vortex lines' motion.

In contrast, ^{3}He is a normal fluid at these temperatures and so may undergo rigid-body rotation. Its angular momentum can change in very small steps of $\hbar$, allowing the drop's total angular momentum to be a dynamical variable. Although ^{3}He is highly viscous at these temperatures, viscosity does not directly damp rigid body rotation.

For both ^{4}He and ^{3}He, the drop's rotational motion is expected to interact with the optical WGMs primarily because the flow field associated with the rotation will deform the drop shape, and thereby detune the WGMs. This coupling would allow optical measurements (i.e., of the WGM) to provide information about the drop's rotational motion. In order to consider the quantum limits of such a measurement, we note that the angular momentum $L_z = I\Omega_z$ is connected to the angular frequency Ω_z via the drop's moment of inertia $I = (8\pi/15)\rho R^5$ (here we assume that the drop is nearly spherical). In principle, Ω_z can be inferred from the WGM detuning caused by the equatorial bulge (which is produced by the centrifugal acceleration $\Omega_z^2 R$). The radius at the equator increases by an amount $\delta R \propto \Omega_z^2$. As described above, the resulting shift of an optical WGM at the equator is $\delta\omega_{\rm opt} = \omega_{\rm opt}\delta R/R$. We thus obtain an optorotational coupling Hamiltonian of the form

$$\hat{H}_{\rm QND} = \hbar g_L \left(\frac{\hat{L}_z}{\hbar}\right)^2 \hat{a}^\dagger \hat{a}\,. \tag{5}$$

The form of this Hamiltonian allows for a QND measurement of $\hat{L}_z^2$.

The Hamiltonian of Eq. (5) is a simplified version of the real coupling, as will be explained in the next section. However, it is sufficient for understanding the basic physics of the optootational coupling, and to estimate the feasibility of angular momentum QND measurements.

The frequency shift g_L in Eq. (5) is given by $g_L = \omega_{\rm opt}(\delta R/R)(\hbar/L_z)^2$, where L_z is the (classical) mean value of the drop's angular momentum and δR is the bulge produced by L_z. By balancing pressure, centrifugal force, and surface tension we find

$$\delta R = (\rho/\sigma) R^4 \Omega_z^2/24. \tag{6}$$

Thus smaller drops deform less for a given angular frequency, due to the smaller centrifugal force. However, in terms of g_L this is overcompensated by the rapidly increasing ratio $\Omega_z/L_z = 1/I$. Altogether, the WGM detuning has a strong dependence on the drop radius:

$$g_L = \omega_{\rm opt} \frac{\hbar^2}{\rho\sigma R^7} \frac{1}{24}\left(\frac{15}{8\pi}\right)^2. \tag{7}$$

Nevertheless, it should be stressed that for typical parameters this constant is exceedingly small. For a ^{3}He drop with $R =$ 1 mm, $\rho \sim 81$ kg/m^3, and $\sigma = 1.52 \times 10^{-4}$ N/m, we have $g_L = \omega_{\rm opt} \times 1.3 \times 10^{-47}$. Fortunately, in most situations the detuning can be much larger than that. This is because the WGM detuning scales with $\hat{L}_z^2$, meaning that changing L_z by $\hbar$ results in a detuning $2g_L(L_z/\hbar)$ and so can be substantially enhanced for large values of $L_z/\hbar$.

In order to detect a given deviation in angular momentum δL_z, a phase shift $\sim\delta\omega_{\rm opt}/\kappa$ has to be resolved by the number of photons $N_{\rm phot}$ sent through the drop's WGM during the time of the measurement. This implies that the minimum detectable phase must be sufficiently small, $\delta\theta = 1/(2\sqrt{N_{\rm phot}}) < \delta\omega_{\rm opt}/\kappa = Q_{\rm opt}\delta\omega_{\rm opt}/\omega_{\rm opt}$. More formally, the resolution is set by $\delta L_z^2 = t_{\rm meas}^{-1} S_L$, where we have introduced the spectral density S_L for the angular momentum imprecision noise. The spectral density is defined in the usual way [76], with $S_L = \int \langle \delta L_z(t)\delta L_z(0)\rangle dt$, where $\delta L_z(t)$ represents the instantaneous fluctuations of the angular momentum deduced from the observed phase shift. Taking into account the phase-shift fluctuations produced by the shot noise of the laser beam, as estimated above, we find

$$S_L \equiv \hbar^2 \left(\frac{\omega_{\rm opt}}{2g_L}\right)^2 \left(\frac{\hbar}{L_z}\right)^2 \left(4Q_{\rm opt}^2 \dot{N}_{\rm phot}\right)^{-1}. \tag{8}$$

We briefly discuss a numerical example to illustrate the possible experimental measurement precision. A normal ^{3}He drop spinning at $\Omega_z/2\pi = 1$ Hz (well below the hydrodynamic instability) will have $L_z/\hbar = I\Omega_z/\hbar = 8 \times 10^{21}$. For $\omega_{\rm opt}/2\pi = 300$ THz ($\lambda = 1$ μm), this yields an optical frequency shift of $2g_L(L_z/\hbar) \approx 2\pi \times 6 \times 10^{-11}$ Hz per $\hbar$ of additional angular momentum. Therefore, we find $\sqrt{S_L} \approx 2 \times 10^{24}\hbar/(Q_{\rm opt}\sqrt{\dot{N}_{\rm phot}})$. For 10 μW of input power and for $Q_{\rm opt} = 10^{10}$, one would thus have an angular momentum resolution of $\sqrt{S_L} \approx 3 \times 10^7 \hbar/\sqrt{\rm Hz}$.

These numbers indicate that it will be impossible to resolve a change of angular momentum by a single quantum $\hbar$. However, one should be able to measure L_z (or L_x or L_y) with a precision better than $\sqrt{\hbar L}$. This is the spread of L_x and L_y in a situation with maximum $L_z = L$, according to Heisenberg's uncertainty relation. Indeed, for the example given above, $\sqrt{\hbar L} \sim 10^{11}\hbar$, which, according to the estimated noise power S_L, can be resolved in $t_{\rm meas} \sim 0.1$ μs. Moreover, in the case of a superfluid ^{4}He drop under identical conditions, the sensitivity $\sqrt{S_L} \approx 1.4 \times 10^8 \hbar/\sqrt{\rm Hz}$ is easily sufficient to carefully monitor a single vortex line, which would carry an angular momentum of $\sim 10^{20}\hbar$.

There are three potential noise sources that may interfere with the QND measurement of angular momentum: fluctuations in the number of evaporating atoms leading to stochastic changes of the drop radius, random angular momentum kicks due to evaporating atoms, and angular momentum transfer by randomly outscattered photons. We have estimated all these effects (see Appendix A), and found them to be smaller than the measurement uncertainty attained in the example given above.

Lastly, we note that in addition to the centrifugal coupling considered above there is also the Fizeau effect, which produces a WGM detuning $\propto\hat{L}_z$ (with a different sign for clockwise and counterclockwise WGM modes). We estimate the single quantum coupling rate for the effect to be $g_F \approx 2\pi \times 10^{-20}$ Hz for $R = 1$ mm. Since the Fizeau effect does not increase with $|L_z|$, we expect the centrifugal coupling to dominate.

B. Coupling between vibrations and rotations

The coupling in Eq. (5) is idealized in two ways. First, it assumes that the drop strictly rotates only around the z axis and that $\hat{L}_x$, $\hat{L}_y$ are not involved in the dynamics. Second, we have written down a direct coupling between rotation and optical frequency. In reality, the rotation will first lead to a deformation, i.e., a displacement of one of the surface modes, and this deformation will then couple to the optical WGM. Conversely, the laser's shot noise will lead to a fluctuating

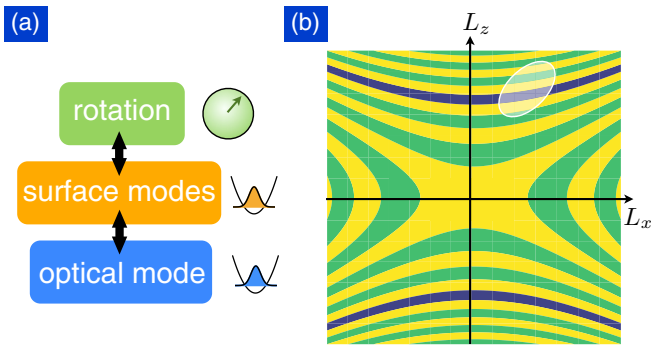

FIG. 6. (a) Nonlinear interactions connect rotational motion to optical frequency shifts via the surface modes. (b) A measurement of the WGM detuning reveals information about $L_z^2 - (L_x^2 + L_y^2)/3$. Contours of this function are shown in the L_x, L_z plane. A given measurement result (within some uncertainty interval) maps to a narrow region (dark blue areas), whose intersection with the state's initial uncertainty (white ellipse) determines the state after the measurement.

force acting on the surface modes, which then couple back to the rotation. This represents the backaction associated with the optical readout.

In the present QND case, the backaction leads to dephasing between different eigenstates of the angular momentum projection $\hat{L}_z$. Physically, fluctuations in the circulating photon number couple to $\hat{L}_z^2$ (via the deformation) which then scramble $\hat{L}_x$ and $\hat{L}_y$.

In summary, a more complete understanding of the optical measurement of angular momentum will require a description of the coupling between mechanical vibrations and the drop's rotations. This is also an interesting dynamical problem in its own right, and it turns the liquid drop into a coupled optomechanical-rotational system [Fig. 6(a)].

The interplay between rotations, deformations, and vibrations in fluid spheres has been studied in nuclear physics (for the liquid drop model of the nucleus [41]), geophysics (for rotating planets), and hydrodynamics (for rotating drops [77]). For small angular frequencies, the two most important effects are (i) the slight deformation of the drop due to the centrifugal force and (ii) a shift in the frequencies of the surface modes. This frequency shift (sometimes known as Bryan's effect [78,79]) is due to the Coriolis force. It leads to a rotation of the surface vibrations that is neither a simple corotation with the rotating drop nor static in the laboratory frame. For the $l = 2$ modes of interest here, the frequencies in the rotating frame are shifted by $-\omega_{\rm rot} m/2$, where m is the mode index ($|m| \leqslant 2$).

Previous studies of the interplay of rotations and vibrations have typically been limited to a fixed rotation axis or other special cases [41,77]. To move beyond these assumptions, we have derived the full Lagrangian of the system without any such assumptions of symmetry, for the case where only $l = 2$ surface modes are excited (extensions to larger l are straightforward). To accomplish this, we note that the surface deformation pattern $\delta R(\theta,\varphi,t)$ in the laboratory frame can be decomposed into spherical harmonics. The five deflection amplitudes X_m of the $l = 2$ surface modes, together with the three Euler rotation angles, form the set of variables in the Lagrangian (Appendix B).

The Lagrangian can be derived by (i) calculating the flow field inside the drop enforced by the time-varying deformation pattern of its surface, (ii) integrating the resulting kinetic energy density over the volume of the drop, and (iii) adding the potential energy from the surface tension. This assumes an incompressible fluid whose flow field can be understood as an irrotational flow pattern in the corotating frame, produced by the surface deformation. The final result involves the deformation variables X_m, the angular velocity vector Ω, and the Euler angles that transform between the corotating frame and the laboratory frame. We display the slightly involved Lagrangian in the Appendixes and we will publish its full derivation elsewhere.

The basic physics can be understood qualitatively by considering the special case of a rotation around the z axis. In particular, the kinetic energy in the Lagrangian contains the following term, beyond the standard terms for the rigid-body rotation of a sphere and the kinetic energies of the surface modes:

$$\frac{I}{4}\sqrt{\frac{5}{\pi}}\frac{X_0}{R}\Omega_z^2. \tag{9}$$

This is the term that couples the bulge mode deflection X_0 to the rotation around the z axis [with the moment of inertia $I = (8\pi/15)\rho R^5$]. Physically, it can be read in two ways. First, spinning up the drop creates a finite deflection proportional to Ω_z^2, which then leads to an optical shift, as discussed previously. Conversely, a deflection increases the moment of inertia and thereby the rotational energy for a given angular frequency.

We note that for a rotating drop there also appears a set of low-frequency modes, the so-called "inertial modes" [80,81]. Their frequencies scale with the rotation frequency, and they are thus well separated from the vibrational modes we have been discussing, as long as the rotation speed is sufficiently far below the instability threshold for nonlinear drop deformation and fission. As a result, we neglect them.

As for the effective coupling between the angular momentum and the optical frequency, we have to point out another interesting aspect that has been omitted in the simplified model of Eq. (5). An optical whispering-gallery mode traveling around the equator in the xy plane will be sensitive not only to the bulge equatorial deformation that is generated by L_z; its frequency will also be shifted by a rotation around the x axis (or y axis), since this leads to an expansion of the equator in the yz (or xz) plane. According to Eq. (2), this frequency shift is 1/3 of that obtained for z rotations and has the opposite sign. As a consequence, the operator that is really measured is expected to be the combination $\hat{L}_z^2 - \frac{1}{3}(\hat{L}_x^2 + \hat{L}_y^2)$. The situation is displayed in Fig. 6(b).

In an experiment, angular momentum will be generated by spinning up the drop (e.g., via the application of a rotating electric field). Such an approach will not select a single energy eigenstate with a definite L, but rather a coherent superposition of various L (as well as of various L_z). The details will depend on the exact procedure used for spinning up the drop, and in practice there will be a thermal incoherent mixture because the experiment is conducted at finite T with a large thermal

population of vibrational and rotational levels. The QND measurements described above would then be able to resolve the angular momentum to some extent, thereby narrowing its distribution via the measurement backaction.

In summary, the Lagrangian that we briefly discussed here will form the general basis for discussions of the intricate coupled nonlinear dynamics of vibrations and rotations in the fluid drop. Among other things, this will enable a detailed analysis of the measurement backaction in optical dispersive measurements of the angular momentum components. However, exploring the rich nonlinear dynamics of this model is beyond the scope of the present work and we leave these steps to future research.

V. OUTLOOK

The levitated helium drop offers a large number of unusual features that represent opportunities for unconventional optomechanics and fundamental studies of superfluid helium physics. Here we will briefly mention some of those.

Due to the large energy of electronic transitions in helium, the drop is expected to handle high circulating optical powers. We estimate the optical spring effect in the drop to be $\sim$1 Hz per photon, so it should be possible to increase the drop's mechanical frequencies by several orders of magnitude. It would remain to be seen how the mechanical Q of a given surface mode would evolve as its frequency is increased past a large number of other mechanical modes. At the same time, the static deflection can remain small ($\sim$1 μm) even for 10^8 circulating photons. Moreover, it would be rather easy in this setup to reach the strong-coupling regime of linearized optomechanics, $g_0 N_{\mathrm{phot}} > \kappa$, for $g_0 \sim 200$ Hz and a conservative estimate of $\kappa \sim 10$ kHz. Thus, using the tools of linear optomechanics [1], one could, e.g., transfer nonclassical optical states into the surface vibrational modes. Possibly, these could then be further transferred onto the angular momentum state, generating optorotational control. Alternatively, the dispersive measurement of angular momentum outlined above can be used to generate interesting postselected states, including states of squeezed angular momentum.

Beyond the conventional linear optomechanical coupling, it should also be possible to realize quadratic coupling in this setup. Indeed, according to Eq. (2), an optical whispering-gallery mode whose plane is tilted at a particular angle will have vanishing linear coupling to the equatorial bulge mode ($l = 2, m = 0$), while the optical WGM in the equatorial plane itself has no linear coupling to the $m \neq 0$ mechanical modes.

In the present manuscript, we have entirely focused on the lowest-order surface vibration modes at $l = 2$. However, one can imagine generating interesting multimode optomechanics when addressing the higher-order modes as well. The collective optical spring effect will be able to generate an effective light-induced interaction between those modes, which can get so strong as to form completely new normal modes. Moreover, one can imagine exploiting transitions between optical modes of different radial and angular momentum quantum numbers. These transitions will then couple efficiently to higher l mechanical modes, e.g., acoustic whispering-gallery modes, leading to Brillouin-like optomechanical interactions [82].

When a drop's surface deformations or rotation rate become sufficiently large, a variety of nonlinear effects are expected to occur. It is known that a rotating drop can develop symmetry-broken shapes [83], but many questions remain open. For example, is it possible to obtain stable drops with nonzero topological genus [84]?

Finally, the optical control and readout can serve as a means to study the physics of superfluid helium in a setting that is devoid of any complications arising from solid surfaces. For example, at low temperatures, the damping of surface waves (ripplons) is due to ripplon-phonon scattering. However, due to the finite size of the drop, the bulk phonons inside the drop constitute a bath with a very strongly frequency-dependent force noise spectrum and strongly non-Markovian properties. These might be studied quantitatively, especially using the optical spring effect as a tool to vary the ripplons' frequency.

Rotation in the superfluid drop is quantized and vortex lines emerge as the drop is made to spin above a certain rotation rate [28,85]. Below that rate, the drop's angular momentum must be contained either in surface modes or in the normal fluid (phonons propagating in the bulk). The presence and the motion of the vortex lines then affects the surface deformation, and this will be readily measurable optically. Even a single vortex line is not inert. It can wiggle, and these vibrations of the stringlike vortex (known as Kelvin modes) could also be read out via their effect on the optical WGM, providing a means for measuring the mechanical properties of an isolated vortex line [86,87]. Moreover, one could investigate the interactions of many vortices as well as quenches through phase transitions, e.g., observing Kibble-Zurek type physics upon cooling a spinning drop. In general, optomechanics in levitated helium drops may become a tool enabling us to explore a whole range of physical phenomena that are analogous to effects in high-energy physics and cosmology [88].

ACKNOWLEDGMENTS

F.M. thanks F. Busse for helpful discussions. F.M., M.S., and A.A. acknowledge support through an ERC Starting Grant ("OPTOMECH"), as well as the European FET proactive network "Hybrid Optomechanical Technologies." L.C. acknowledges support from a L'Oreal USA FWIS Fellowship (2012), NSERC Discovery No. 435554-2013, and a Canada Research Chairs Grant No. 950-229003. J.H. acknowledges support from W. M. Keck Foundation Grant No. DT121914, AFOSR Grants No. FA9550-09-1-0484 and No. FA9550-15-1-0270, DARPA Grant No. W911NF-14-1-0354, ARO Grant No. W911NF-13-1-0104, and NSF Grant No. 1205861. This work has been supported by the DARPA/MTO ORCHID Program through a grant from AFOSR. This project was made possible through the support of a grant from the John Templeton Foundation. This material is based upon work supported by the National Science Foundation Graduate Research Fellowship under Grant No. DGE-1122492.

APPENDIX A: NOISE SOURCES FOR THE QND MEASUREMENT OF ANGULAR MOMENTUM

There are three noise sources that may potentially interfere with the QND measurement of the drop's angular momentum.

The first is due to the fact that the evaporation of atoms is a stochastic process. When N atoms evaporate on average during a given time interval, that number actually fluctuates by $\sqrt{N}$, leading to corresponding fluctuations in the drop radius and the optical resonance. The effect diminishes as the temperature decreases and the evaporation rate slows. The relevant rates can be extracted from Fig. 5. After 1000 s of evaporation, a ^{3}He drop reaches $T \approx 0.13$ K with $\sim$1 nW of cooling power. This corresponds to 4×10^{13} atoms evaporating per second, with a resulting deterministic drift of the optical resonance of $\sim$60 MHz/s. In Sec. III A we considered a measurement time of 0.1 μs, which is sufficiently long to resolve an angular momentum spread of the order of the Heisenberg uncertainty, $\sqrt{\hbar L}$. During this time, the number of evaporated atoms fluctuates only by about 10^3, leading to a negligible stochastic optical shift of $\sim 10^{-3}$ Hz.

The second noise source is directly connected to the same physics: the evaporating atoms will also carry away angular momentum. For $T = 0.1$ K, a single atom flying off with the mean thermal velocity can extract $\sim 10^6\hbar$ from a droplet of radius $R = 1$ mm. Staying with the example considered in the previous paragraph, in 0.1 μs this results in a stochastic contribution to L_z of $10^9\hbar$, much smaller than the $10^{11}\hbar$ measurement resolution mentioned above.

Finally, the third noise source is present even in the absence of evaporation. It consists of changes in the drop's angular momentum due to the scattering of photons. Each randomly scattered photon can carry away angular momentum $\sim R\hbar k$, which amounts to about $6000\hbar$. Assuming an input power of 10 μW and that 10% of the photons are scattered stochastically in random directions (e.g., from the thermal surface fluctuations), this process would result in a stochastic angular momentum transfer (during a 0.1 μs measurement time) of $\sim 4 \times 10^6\hbar$, well below the measurement uncertainty.

APPENDIX B: LAGRANGIAN FOR THE COUPLING OF ROTATIONS TO THE $l = 2$ VIBRATIONS IN AN INCOMPRESSIBLE FLUID DROP

The purpose of this Appendix is to display the full Lagrangian describing the coupling between arbitrary rotations and the vibrational $l = 2$ surface modes of the drop. To that end, we have to introduce a number of definitions. The derivation of this Lagrangian will be discussed in a separate publication (see also the thesis in Ref. [42]).

For brevity, it is convenient from now on to measure lengths in units of the sphere radius (such that $R = 1$). Appropriate dimensions can be reinstated later, if needed. The surface deformation pattern in the laboratory frame is given by

$$\delta R^{\mathrm{Lab}}(\mathbf{r},t) = \sum_{m=-2}^{2} X_m^{\mathrm{Lab}}(t)\phi_m(\mathbf{r}), \tag{B1}$$

where $\mathbf{r}$ resides on the surface ($|\mathbf{r}| = 1$). The $\phi_m(\mathbf{r})$ are based on the $l = 2$ spherical harmonics, $\phi_m(\mathbf{r}) \sim r^2 Y_{l,m}(\theta,\phi)$. They have been extended to cover all of space, which will simplify the notation further below. More precisely, we have defined $\phi_{\pm 2} = \mathcal{N}_2(x \pm iy)^2$, $\phi_{\pm 1} = \mathcal{N}_1(x \pm iy)z$, and $\phi_0 = \mathcal{N}_0(x^2 + y^2 - 2z^2)$; where the constants are $\mathcal{N}_2 = (32\pi/15)^{-1/2}$, $\mathcal{N}_1 = (8\pi/15)^{-1/2}$, and $\mathcal{N}_0 = (16\pi/5)^{-1/2}$. The surface integrals are normalized, $\int |\phi_m|^2 \sin\theta\, d\theta\, d\varphi = 1$ for $|\mathbf{r}| = 1$.

To write down the Lagrangian, we need to convert between the laboratory frame and the corotating frame (described by a set of three Euler angles which we sometimes combine into a three-vector $\vec{\varphi}$). We assume that the transformation is effected by a suitable 5×5 matrix W, with $X^{\mathrm{Lab}} = W X^{\mathrm{Rot}}$, or explicitly

$$X_m^{\mathrm{Lab}} = \sum_{m=-2}^{2} W_{mm'}(\vec{\varphi}) X_m^{\mathrm{Rot}}. \tag{B2}$$

Upon rotation of the drop by the angular frequency vector Ω (which is expressed in the laboratory frame), the matrix W changes according to

$$\frac{d}{dt} W_{mm'} = -\sum_{s=1}^{3} \sum_{k=-2}^{2} \Omega_s K_{km}^{(s)} W_{km'}, \tag{B3}$$

or $\dot{W} = -\sum_s \Omega_s (K^{(s)})^t W$ in matrix notation. This relation defines the generators $K_{km}^{(s)}$ that describe infinitesimal rotations. The generator $K^{(3)}$ for rotations around the z axis is the simplest one, with $K_{km}^{(3)} = im\delta_{k,m}$. Finally, we introduce the notation $D_m^{\mathrm{Rot}} = X_m^{\mathrm{Rot}}$ and $D^{\mathrm{Lab}} = W D^{\mathrm{Rot}}$. With these definitions, we are now in a position to write down the full Lagrangian that couples vibrations and rotation:

$$\begin{aligned}\mathcal{L} = {} & \frac{I}{2}\Omega^2 + \frac{\rho}{4}\dot{X}_m^{\mathrm{Rot}*}\dot{X}_m^{\mathrm{Rot}} - \frac{I}{2}\delta R^{\mathrm{Lab}}(\Omega) \\ & + \frac{\rho}{4} D_m^{\mathrm{Lab}} \Omega_s K_{mm'}^{(s)} X_{m'}^{\mathrm{Lab}*} - 2\sigma X_m^{\mathrm{Rot}*} X_m^{\mathrm{Rot}}.\end{aligned} \tag{B4}$$

Summation over repeated indices is implied. This Lagrangian contains, in this order, (i) the rotational energy of the unperturbed spherical drop, (ii) the kinetic energy of the surface vibrations, (iii) the change in the rotational energy due to the deformation (with the surface deformation field δR evaluated at the angular momentum vector), (iv) the term describing Bryan's effect (from the Coriolis force), and (v) the potential energy of the surface vibrations (due to the surface tension). We note that all the deformation-related quantities (X^{Rot}, X^{Lab}, and D^{Lab}) have to be expressed via X^{Rot} for the purpose of deriving the equations of motion. We also note that the X^{Rot} coefficients obey the constraint $X_{-m}^{\mathrm{Rot}} = X_m^{\mathrm{Rot}*}$ due to the fact that the surface deformation is real valued. In deriving the equations of motion, one can either split X_m^{Rot} into real and imaginary parts (for $m > 0$) or, more efficiently, formally treat X_m^{Rot} and $X_m^{\mathrm{Rot}*}$ as independent variables.

[1] M. Aspelmeyer, T. J. Kippenberg, and F. Marquardt, Rev. Mod. Phys. **86**, 1391 (2014).

[2] A. D. O'Connell, M. Hofheinz, M. Ansmann, R. C. Bialczak, M. Lenander, E. Lucero, M. Neely, D. Sank, H. Wang, M. Weides, A. N. Cleland, and J. M. Martinis, Nature (London) **464**, 697 (2010).

[3] N. Brahms, T. Botter, S. Schreppler, D. W. C. Brooks, and D. M. Stamper-Kurn, Phys. Rev. Lett. **108**, 133601 (2012).

[4] A. B. Shkarin, A. D. Kashkanova, C. D. Brown, S. Garcia, K. Ott, J. Reichel, and J. G. E. Harris, arXiv:1709.02794 (2017).

[5] T. P. Purdy, K. E. Grutter, K. Srinivasan, and J. M. Taylor, Science **356**, 1265 (2017).

[6] M. Underwood, D. Mason, D. Lee, H. Xu, L. Jiang, A. B. Shkarin, K. Børkje, S. M. Girvin, and J. G. E. Harris, Phys. Rev. A **92**, 061801 (2015).

[7] I. Pikovski, M. R. Vanner, M. Aspelmeyer, M. S. Kim, and C. Brukner, Nat. Phys. **8**, 393 (2012).

[8] H. Yang, H. Miao, D.-S. Lee, B. Helou, and Y. Chen, Phys. Rev. Lett. **110**, 170401 (2013).

[9] O. Romero-Isart, Phys. Rev. A **84**, 052121 (2011).

[10] D. E. Chang, C. A. Regal, S. B. Papp, D. J. Wilson, J. Ye, O. Painter, H. J. Kimble, and P. Zoller, Proc. Natl. Acad. Sci. USA **107**, 1005 (2010).

[11] O. Romero-Isart, M. L. Juan, R. Quidant, and J. I. Cirac, New J. Phys. **12**, 033015 (2010).

[12] P. F. Barker and M. N. Shneider, Phys. Rev. A **81**, 023826 (2010).

[13] J. Millen, T. Deesuwan, P. Barker, and J. Anders, Nat. Nanotechnol. **9**, 425 (2014).

[14] T. Li, S. Kheifets, D. Medellin, and M. G. Raizen, Science **328**, 1673 (2010).

[15] T. Li, S. Kheifets, and M. G. Raizen, Nat. Phys. **7**, 527 (2011).

[16] O. Romero-Isart, A. C. Pflanzer, F. Blaser, R. Kaltenbaek, N. Kiesel, M. Aspelmeyer, and J. I. Cirac, Phys. Rev. Lett. **107**, 020405 (2011).

[17] J. Gieseler, B. Deutsch, R. Quidant, and L. Novotny, Phys. Rev. Lett. **109**, 103603 (2012).

[18] K. W. Murch, K. L. Moore, S. Gupta, and D. M. Stamper-Kurn, Nat. Phys. **4**, 561 (2008).

[19] F. Brennecke, S. Ritter, T. Donner, and T. Esslinger, Science **322**, 235 (2008).

[20] R. Dahan, L. L. Martin, and T. Carmon, Optica **3**, 175 (2016).

[21] G. Bahl, K. H. Kim, W. Lee, J. Liu, X. Fan, and T. Carmon, Nat. Commun. **4**, 1994 (2013).

[22] A. D. Kashkanova, A. B. Shkarin, C. D. Brown, N. E. Flowers-Jacobs, L. Childress, S. W. Hoch, L. Hohmann, K. Ott, J. Reichel, and J. G. E. Harris, Nat. Phys. **13**, 74 (2017).

[23] A. D. Kashkanova, A. B. Shkarin, C. D. Brown, N. E. Flowers-Jacobs, L. Childress, S. W. Hoch, L. Hohmann, K. Ott, J Reichel, and J. G. E. Harris, J. Opt. **19**, 034001 (2017).

[24] L. A. D. Lorenzo and K. C. Schwab, New J. Phys. **16**, 113020 (2014).

[25] G. I. Harris, D. L. McAuslan, E. Sheridan, Y. Sachkou, C. Baker, and W. P. Bowen, Nat. Phys. **12**, 788 (2016).

[26] S. Singh, L. A. De Lorenzo, I. Pikovski, and K. C. Schwab, New J. Phys. **19**, 073023 (2017).

[27] L. F. Gomez *et al.*, Science **345**, 906 (2014).

[28] G. H. Bauer, R. H. Donnelly, and W. F. Vinen, J. Low Temp. Phys. **98**, 47 (1995).

[29] M. A. Weilert, D. L. Whitaker, H. J. Maris, and G. M. Seidel, Phys. Rev. Lett. **77**, 4840 (1996).

[30] M. A. Weilert, D. L. Whitaker, H. J. Maris, and G. M. Seidel, J. Low Temp. Phys. **106**, 101 (1997).

[31] C. Vicente, W. Yao, H. J. Maris, and G. M. Seidel, Phys. Rev. B **66**, 214504 (2002).

[32] J. P. Toennies and A. F. Vilesov, Angew. Chem., Int. Ed. **43**, 2622 (2004).

[33] H.-M. Tzeng, K. F. Wall, M. B. Long, and R. K. Chang, Opt. Lett. **9**, 499 (1984).

[34] H.-M. Tzeng, P. W. Barber, M. B. Long, and R. K. Chang, Opt. Lett. **10**, 209 (1985).

[35] S.-X. Qian, J. B. Snow, H.-M. Tzeng, and R. K. Chang, Science **231**, 486 (1986).

[36] M. Tanyeri, R. Perron, and I. M. Kennedy, Opt. Lett. **32**, 2529 (2007).

[37] S. Uetake, M. Katsuragawa, M. Suzuki, and K. Hakuta, Phys. Rev. A **61**, 011803 (1999).

[38] S. Uetake, R. S. D. Sihombing, and K. Hakuta, Opt. Lett. **27**, 421 (2002).

[39] A. N. Oraevsky, Quantum Electron. **32**, 377 (2002).

[40] L. Rayleigh, Proc. R. Soc. London **29**, 71 (1879).

[41] A. Bohr and B. R. Mottelson, *Nuclear Structure Vol. II: Nuclear Deformations* (World Scientific, Singapore, 1998).

[42] M. Schmidt, Ph.D. thesis, University Erlangen-Nuremberg, Erlangen, 2015 (unpublished).

[43] H. Gang, A. H. Krall, and D. A. Weitz, Phys. Rev. E **52**, 6289 (1995).

[44] H. M. Lai, P. T. Leung, K. Young, P. W. Barber, and S. C. Hill, Phys. Rev. A **41**, 5187 (1990).

[45] R. J. A. Hill and L. Eaves, Phys. Rev. E **81**, 056312 (2010).

[46] D. L. Whitaker, C. Kim, C. L. Vicente, M. A. Weilert, H. J. Maris, and G. M. Seidel, J. Low Temp. Phys. **113**, 491 (1998).

[47] D. L. Whitaker, C. Kim, C. L. Vicente, M. A. Weilert, H. J. Maris, and G. M. Seidel, J. Low Temp. Phys. **114**, 523 (1999).

[48] R. W. Whitworth, Proc. R. Soc. London, A **246**, 390 (1958).

[49] H. J. Maris, Phys. Rev. A **8**, 1980 (1973).

[50] R. Webeler and D. Hammer, Phys. Lett. **19**, 533 (1965).

[51] R. Webeler and D. Hammer, NASA Technical Note D-4381, Technical Report, 1968 (unpublished).

[52] P. Roche, M. Roger, and F. I. B. Williams, Phys. Rev. B **53**, 2225 (1996).

[53] S. Chandrasekhar, Proc. London Math. Soc. **s3**, 141 (1959).

[54] D. S. Betts, D. W. Osborne, B. Welber, and J. Wilks, Philos. Mag. **8**, 977 (1963).

[55] D. S. Betts, B. E. Keen, and J. Wilks, Proc. R. Soc. London, A **289**, 34 (1965).

[56] J. Popp, M. H. Fields, and R. K. Chang, Opt. Lett. **22**, 1296 (1997).

[57] J. P. R. Lacey and F. P. Payne, IEEE Proc. J: Optoelectron. **137**, 282 (1990).

[58] M. L. Gorodetsky, A. D. Pryamikov, and V. S. Ilchenko, JOSA B **17**, 1051 (2000).

[59] G. M. Seidel, R. E. Lanou, and W. Yao, Nucl. Instrum. Methods, Phys. Res. A **489**, 189 (2002).

[60] M. A. Weilert, D. L. Whitaker, H. J. Maris, and G. M. Seidel, J. Low Temp. Phys. **98**, 17 (1995).

[61] T. J. Greytak and J. Yan, Phys. Rev. Lett. **22**, 987 (1969).

[62] D. M. Brink and S. Stringari, Z. Phys. D **15**, 257 (1990).

[63] For ^{4}He vapor pressure at temperatures below 0.65 K, we use the theoretical Arrhenius law for evaporation rate [62], which fits

experimental data well even at more elevated temperatures. All other values are found by interpolating published experimental data or using published empirical formulas within their region of validity.

[64] R. J. Donnelly and C. F. Barenghi, J. Phys. Chem. Ref. Data **27**, 1217 (1998).
[65] D. S. Greywall, Phys. Rev. B **27**, 2747 (1983).
[66] E. C. Kerr, Phys. Rev. **96**, 551 (1954).
[67] Y. H. Huang and G. B. Chen, Cryogenics **46**, 833 (2006).
[68] B. A. Stickler, B. Papendell, and K. Hornberger, Phys. Rev. A **94**, 033828 (2016).
[69] B. A. Stickler, S. Nimmrichter, L. Martinetz, S. Kuhn, M. Arndt, and K. Hornberger, Phys. Rev. A **94**, 033818 (2016).
[70] S. Kuhn, B. A. Stickler, A. Kosloff, F. Patolsky, K. Hornberger, M. Arndt, and J. Millen, Nat. Commun. **8**, 1670 (2017).
[71] S. Kuhn, A. Kosloff, B. A. Stickler, F. Patolsky, K. Hornberger, M. Arndt, and J. Millen, Optica **4**, 356 (2017).
[72] S. Liu, T. Li, and Z.-Q. Yin, JOSA B **34**, C8 (2017).
[73] T. M. Hoang, Y. Ma, J. Ahn, J. Bang, F. Robicheaux, Z.-Q. Yin, and T. Li, Phys. Rev. Lett. **117**, 123604 (2016).
[74] C. C. Rusconi, V. Pöchhacker, K. Kustura, J. I. Cirac, and O. Romero-Isart, Phys. Rev. Lett. **119**, 167202 (2017).
[75] C. C. Rusconi and O. Romero-Isart, Phys. Rev. B **93**, 054427 (2016).
[76] A. A. Clerk, M. H. Devoret, S. M. Girvin, F. Marquardt, and R. J. Schoelkopf, Rev. Mod. Phys. **82**, 1155 (2010).
[77] F. H. Busse, J. Fluid Mech. **142**, 1 (1984).
[78] G. H. Bryan, Proc. Cambridge Philos. Soc., Math and Phys. Sci. VII, 101 (1890).
[79] S. V. Joubert, M. Y. Shatalov, and T. H. Fay, Am. J. Phys. **77**, 520 (2009).
[80] H. P. Greenspan, *The Theory of Rotating Fluids* (CUP Archive, Cambridge, UK, 1968), google-Books-ID: 2R47AAAAIAAJ.
[81] L. D. Landau and E. M. Lifshitz, *Fluid Mechanics* (Elsevier, Amsterdam, 2013), google-Books-ID: CeBbAwAAQBAJ.
[82] G. Bahl, M. Tomes, F. Marquardt, and T. Carmon, Nat. Phys. **8**, 203 (2012).
[83] R. J. A. Hill and L. Eaves, Phys. Rev. Lett. **101**, 234501 (2008).
[84] C.-J. Heine, IMA J. Numer. Anal. **26**, 723 (2006).
[85] G. M. Seidel and H. J. Maris, Physica B **194**, 577 (1994).
[86] W. F. Vinen, M. Tsubota, and A. Mitani, Phys. Rev. Lett. **91**, 135301 (2003).
[87] E. Kozik and B. Svistunov, Phys. Rev. Lett. **92**, 035301 (2004).
[88] G. E. Volovik, *The Universe in a Helium Droplet*, 1st ed. (Oxford University Press, Oxford, 2009).